

**2023 NDIA MICHIGAN CHAPTER  
GROUND VEHICLE SYSTEMS ENGINEERING  
AND TECHNOLOGY SYMPOSIUM  
MODELING, SIMULATION AND SOFTWARE (MS2) TECHNICAL SESSION  
AUGUST 15-17, 2023 - NOVI, MICHIGAN**

**ADAPTATION OF THE DYNAMIC MODE DECOMPOSITION  
METHODOLOGY TO HIGH REYNOLDS NUMBER FLOW OVER A  
GROUND VEHICLE : CHALLENGES AND MITIGATION**

**Adit Misar, PhD<sup>1</sup>, Spencer Nichols<sup>1</sup>, Vamshi M. Korivi, PhD<sup>2</sup>, Nathan A. Tison,  
PhD<sup>2</sup>, Mesbah Uddin, PhD<sup>1\*</sup>**

<sup>1</sup>Mechanical Engineering, University of North Carolina at Charlotte, NC

<sup>2</sup>US Army DEVCOM – Ground Vehicle Systems Center, Warren, MI

\*Corresponding Author

**ABSTRACT**

*The Dynamic Mode Decomposition (DMD) has shown the ability to extract coherent structures and dominant modes from high dimensional, sequential flow field datasets by decomposing it into spatial patterns and associated time dynamics. This low-rank dataset can then be applied to a linear regression model to predict the future state of the flow. Additionally, the DMD with control (DMDc) algorithm enables the input of control signals to the system, a very promising avenue for developing active aero devices for ground and aerial vehicles. However, existing literature primarily consists of its applications to low Reynolds number flows past simple, and mostly two-dimensional geometries. Given that most flows of engineering interest involve three-dimensional turbulent flows having high Reynolds number, this paper explores and presents DMD analyses of the flow around an idealized ground vehicle (Ahmed body) at a Reynolds number of 2.7 million. The high dimensional dataset for this paper was generated using numerical simulations, i.e. Computational Fluid Dynamics (CFD). Based on the success of the hybrid turbulence modeling methodology, called the Improved Delayed Detached Eddy Simulation or IDDES, in predicting external flows past generic road vehicles, all simulations used in this paper were carried out using the IDDES approach. We observed that for such a complex and high Reynolds number flow, application of the DMD algorithms, as can be found in existing literature, failed to meet the desired objective of obtaining reliable reduced-order-model predictions of the flow fields. This necessitates enhancements to the existing algorithm to be explored, and thus, a modified DMD algorithm*

*applicable to high Reynolds number, separation-dominated flows was developed and presented in this paper. The veracity of the modified DMD-based data-dimensionality reduction approach was tested by comparing the mean values, the root-mean-squared (RMS) values, and power spectral density (PSD) of force and moment coefficients that were obtained from the reconstruction of the surface-pressure field using the DMD-based reduced order model to true CFD simulation data.*

**Citation:** A. Misar, S. Nichols, V. Korivi, N. Tison and M. Uddin, "Adaptation of the Dynamic Mode Decomposition Methodology to High Reynolds Number Flow over a Ground Vehicle : Challenges and Mitigation," In *Proceedings of the Ground Vehicle Systems Engineering and Technology Symposium (GVSETS)*, NDIA, Novi, MI, Aug. 15-17, 2023.

## 1 INTRODUCTION

Fluid flows at high Reynolds numbers are complex as they consist of vortical structures that exhibit a wide range of length and time scales [1, 2]. The intricate dynamics of the turbulent structures present a challenge concerning their understanding and analysis [3, 4]. Such types of flows are common in engineering systems, such as external aerodynamic flows around aircraft and vehicles [5, 6]. Another interesting type of flow can be seen in the case of a train of vehicles in a platoon, where the aerodynamic characteristics of a platoon member involves a complex interaction of the flow over the platoon member itself as well as the flow over the preceding and proceeding vehicles [7]. Yet another frontier of recent times is the autonomous landing of Unmanned Aerial Vehicles (UAV) on moving ground vehicles (GV). In this case, the flow fields around both the UAV and GV interact when they are in close proximity of each other. This interaction makes the turbulent flow exhibit even more unpredictable behavior, and adds to the challenge of extracting relevant information to identify the coherent flow patterns [5, 8]. Thus, accurate prediction

of these flows is critical for active flow control, optimizing the aerodynamic drag and/or improving the vehicle's aerodynamic stability [9, 10]. Further, this is extremely important in the field of autonomous systems, as will be discussed later.

Traditionally, the investigations of high Reynolds number flows relied heavily on experimental measurements [3, 11] as the accurate numerical computation of these complex flows using currently available Computational Fluid Dynamics (CFD) tools like Direct Numerical Simulations (DNS), or Large Eddy Simulations (LES) remains computationally prohibitive [12, 13]. However, significant progress has been made in this field such that CFD has established itself as a first-order approximation tool in the aerodynamic development of ground vehicles (c.f. [9, 14, 15, 16, 17, 10]). Additionally, scale-resolved CFD simulation methodologies, like the Detached Eddy Simulation (DES) approaches, have shown promising results in resolving the transient flow field around a ground vehicle [7, 18, 19]. While a detailed and reliable flow prediction is achievable using DES methods, the requirement of immense

---

DISTRIBUTION A. Approved for public release; distribution unlimited. OPSEC # 7352.

computational resources still remains. This is prohibitive as the onboard controller on a moving vehicle may not have the processing power and/or time needed to solve a transient flow field while attempting to implement real-time control of the vehicle's trajectory. Consequently, there is a growing need for alternative approaches that can capture the underlying dynamics of these complex flows more efficiently. One alternative approach is to develop a Reduced Order Model (ROM) to obtain sufficiently accurate flow predictions while using reasonable computational resources; this objective is the driving force behind looking into the feasibility of various surrogate models which can be computationally inexpensive, yet accurate and reliable [20, 21]. In recent years, the Dynamic Mode Decomposition (DMD) algorithm has emerged as a promising data-driven methodology for extracting coherent structures and capturing the spatio-temporal behavior of fluid flows. DMD can decompose a set of high-dimensional data into its low-dimensional constituent modes and extract the associated oscillation frequencies, amplitudes, and growth rates of each mode [22]. These constituent modes and their associated oscillation frequencies can then be used to make future state predictions of the system [23, 24]; additionally, a control signal may be added to the decomposed flow field [25].

Performing DMD is a step-by-step process, and readers are directed to Kutz's book [26] and Schmid's review paper [27] for the detailed description. However, for the readers' benefit, the steps required to perform a DMD analysis are reviewed below.

[1] Collect multiple time snapshots of the system of interest,

- [2] Create a low-dimensional subspace using the Singular Value Decomposition (SVD) or Truncated SVD (TSVD),
- [3] Obtain an eigendecomposition of the low-dimensional subspace,
- [4] Using the eigendecomposition, assemble the mode shapes and their associated oscillation frequencies, called the 'Time Dynamics' or TD for short,
- [5] Use the mode shapes and TD to assemble the output equation.

DMD has been successfully applied to a range of fluid flow problems at low [24, 28, 29] to moderate Reynolds numbers [30, 31]. However, despite its successes, the adaptation of DMD to high Reynolds number, complex, separation-dominated flows remains a challenging task, such as the flow over a Ground Vehicle (GV) [20, 21]. The inherent complexity and turbulence characteristics of such flows introduce additional difficulties in accurately identifying and capturing the underlying coherent structures. Ahani and Uddin (2022) [20] performed DMD on a DrivAer geometry, which is a simplified vehicle geometry, at a Reynolds number of  $4.8 \times 10^6$ ; however, their work primarily focused on comparing the obtained mode shapes from DMD to those obtained from other classical decomposition methods like the Proper Orthogonal Decomposition (POD). Another study with the DrivAer geometry, presented by Matsumoto (2017) [32], performed a low-pass filtering with a cutoff frequency of 10 Hz before the data was sent to the DMD algorithm [32]. Consequently, this work filtered out all the complexities associated with a high Reynolds number flow. Thus, the objective of this paper is to present an investigation into the adaptation of the DMD

methodology specifically for high Reynolds number flows.

Given this background, this paper aims to study some key aspects that are critical to the successful performance of the DMD algorithm when applied to the flow field of a moving ground vehicle corresponding to a high Reynolds number flow. These aspects include the selection and pre-processing of the flow data, the temporal sampling rate, the truncation criteria, and spectral analysis of the predictions, which are crucial for obtaining accurate and reliable results. When it comes to the question of developing a ROM, the potential of utilizing DMD as the ROM technique for high Reynolds number flows will be explored. The key aspects are summarized below for the readers' benefit:

- How many samples of data are required?
- What is the physical time period for each sample?
- What are the desired CFD time-stepping and DMD data collection frequency?
- What are the truncation criteria for the SVD?
- Is there a need to remove spurious modes from the obtained decomposition?
- How much of the flow energy is conserved when the flow field is reconstructed?
- What is the minimum energy that must be retained when performing a low-dimensional transformation of the system?

This paper will attempt to address the above fundamental questions pertaining to the DMD analyses of high Reynolds number, separation-dominated flows. A modified

DMD framework that was developed as part of this work will be presented as a practical guideline capable of capturing the underlying dynamics of high Reynolds number flow around a moving ground vehicle. This study used the Ahmed body geometry [33] as the model of an idealized road vehicle. The slant angle of the Ahmed body was chosen as  $35^{\circ}$  as it exhibits the characteristic flow features of an SUV-type vehicle, such as a humvee, which is the focus of the next phase of our work [5]. By leveraging recent advancements in computational techniques, the CFD simulations were carried out using the transient Improved Delayed Detached Eddy Simulation (IDDES) turbulence modeling method proposed by Shur et al. [34].

## 2 CFD SETUP

The full-scale geometry was placed inside a Virtual Wind Tunnel (VWT) having the same dimensions as Ahmed's [33] original wind tunnel experiment ( $8L$ ,  $5H$ , and  $5W$  stream-wise, vertical and lateral extents, respectively); this results in a blockage ratio of about 4%. A schematic of the setup can be seen in Fig 1 (Top) which also contains the coordinate system and the dimensions. A velocity inlet of 40 m/s was applied to the upstream face with a turbulence intensity of 0.25% and a turbulence length scale of 10 mm; a 0 Pa gauge pressure was applied to the downstream face. All other boundaries were treated as no-slip walls for computational efficiency.

However, the wind tunnel setup described above necessitates blockage ratio corrections. Since most vehicles operate in open-air (OA) conditions, the simulation was adapted accordingly. To do this the domain extents were significantly increased and the side wall boundaries were changed to a velocity inlet

and a pressure outlet to prepare for crosswind simulations which will be the subject of a subsequent study. Additionally, to imitate a moving-ground simulation, the floor of the tunnel was given a tangential velocity equal to the free-stream velocity. This setup was taken from the authors' experience of performing CFD crosswind simulations involving road vehicles [14, 18, 19]. The updated VWT domain can be seen in Fig. 1 (Bottom).

The simulation domain is discretized using unstructured hexahedral cells. To properly resolve the flow around the GV, five refinement volumes were used around the geometry. The finest mesh had a size of the Taylor length scale. Further, to properly resolve the boundary layer flows on all the surfaces, a prism layer mesher was used to ensure that the wall-node  $y^+$  values are less than unity ( $y^+ \equiv yu_\tau/\nu$ , where  $y$ ,  $u_\tau$ , and  $\nu$  are the surface-normal distance, friction velocity, and fluid kinematic viscosity, respectively). Fig 2 (Top) shows the central-plane view (at  $y = 0$ ) of the final mesh of 15.24 million cells in which more than 99% surfaces had a  $y^+$  value less than unity. For the open-air domain, the meshing parameters were kept the same as the WT domain case except that prism layers were disabled on the far field walls. The new mesh can be seen in Fig 2 (Bottom) and consists of 21.94 million cells.

Simulations were carried out using a commercial finite volume code Simcenter Star-CCM+ developed by Siemens Digital Industries Software. The SST Menter  $k - \omega$  (SST) [35, 36] based incompressible IDDES approach was used as the solver. A two-layer wall treatment was used to ensure accurate boundary layer simulation. The time step size of  $\Delta t = 2.5 \times 10^{-4}s$

was found to be sufficient for this setup [37, 38] to produce time-step-independent, and reliable results. Each time step included 10 inner iterations to ensure that residuals reduced by at least 3 orders of magnitude. To minimize the effects of domain decomposition in CFD predictions, all simulations were run on UNC Charlotte High Performance Computing (HPC) clusters using 144 processors across 3 nodes having 48 processors each [39]. The simulation's physical end time was 160 LETOTs where the last 80 LETOTs were used for averaging and data collection. Note that 1 Large Eddy Turn Over Time (LETOT) is defined as  $LETOT = L/U_\infty$ , where  $L$  and  $U_\infty$  stand for the vehicle characteristic length, and free-stream velocity, respectively.

### 3 CFD VALIDATION

CFD prediction from this work was validated for drag coefficient ( $C_D$ ) computations against the wind tunnel measurements of Ahmed [33], and IDDES CFD simulation of Guilmineau et al. [37]. This comparison is shown in Fig. 3 which also contains predictions using the OA configuration. Clearly, the drag predictions of the proposed CFD methodology match very well with the experimental results when the vehicle is placed in a wind tunnel domain. The VWT in OA configuration has a blockage ratio of less than 0.25%. As such up to 12% drop in  $C_D$  prediction can be expected [40, 41]. The drop in  $C_D$  observed is 6.3%.

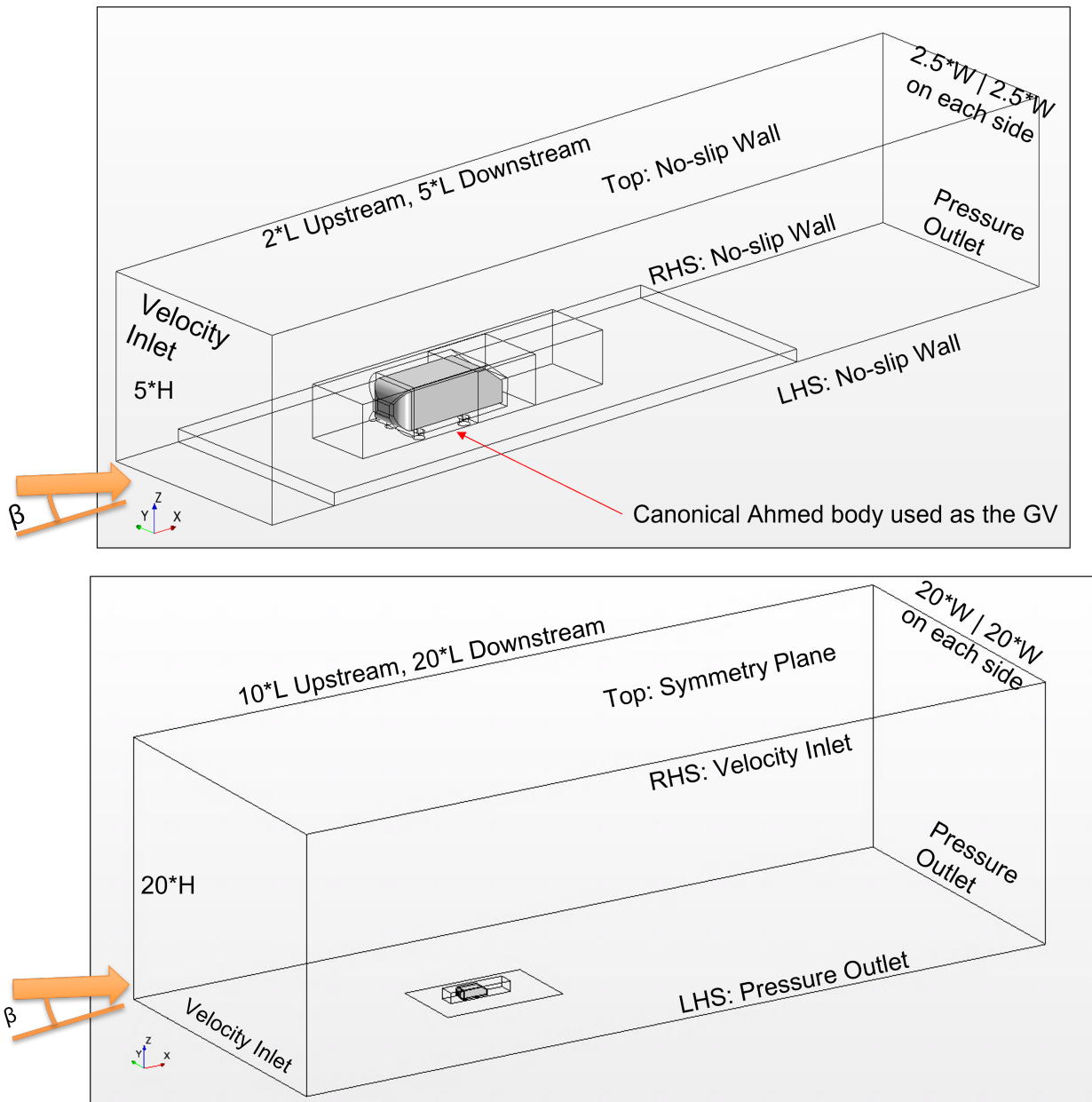


Figure 1: Ahmed body in Wind Tunnel (Top) and Open-air (Bottom) domains.

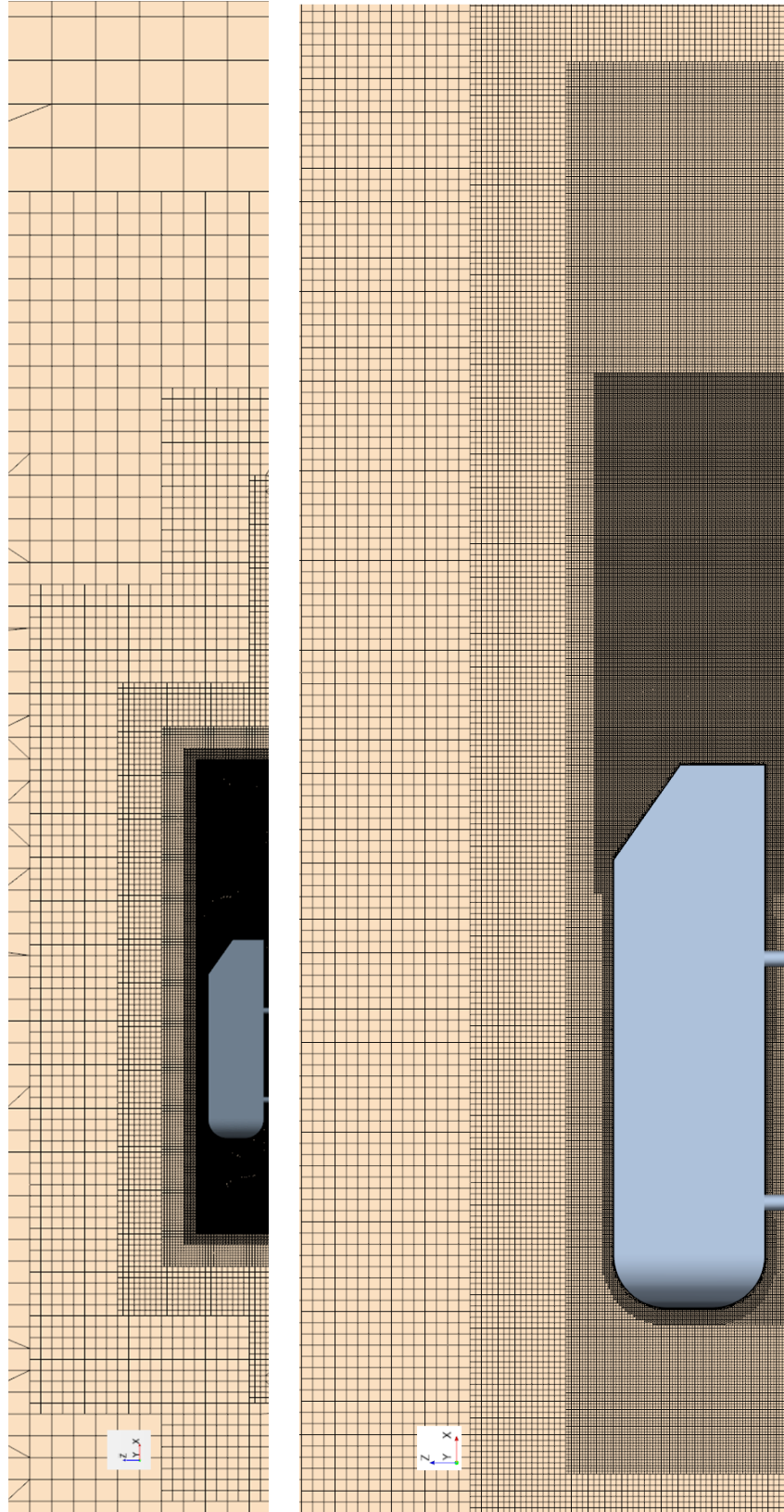


Figure 2: Mesh used for simulating the Ahmed body in Wind Tunnel (Top), and Open-Air (Bottom) domains.

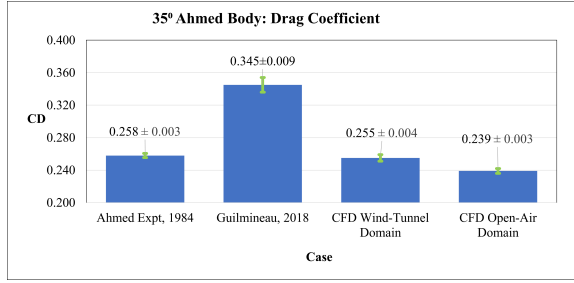


Figure 3: Validation of the CFD setup

#### 4 MATHEMATICAL FRAMEWORK OF THE DYNAMIC MODE DECOMPOSITION

First step in the DMD process involves storing the time-series data in a vector form,  $X_i = \{x_i^1, x_i^2, \dots, x_i^n\}$ , where the subscript  $i$  represents the  $i^{\text{th}}$  element of the grid. The superscripts  $j = 1, 2, \dots, n$  represent the  $j^{\text{th}}$  instantaneous time-snapshots of the flow-field at location  $x_i$ ; here  $n$  is the total number of time snapshots collected. Thus, each time snapshot  $x^j$ , is a column vector containing data from all the  $m$  grid elements at time instant  $j$ . If we expand the vectors for the grid elements, we then can build the complete dataset in a matrix form; this is shown in equation 1.

$$X = \begin{bmatrix} x_1^1 & x_1^2 & \dots & x_1^n \\ \vdots & \vdots & \ddots & \vdots \\ x_m^1 & x_m^2 & \dots & x_m^n \end{bmatrix} \quad (1)$$

The idea is to represent this data of a non-linear, complex system as a locally linear regression such that  $x_{k+1} = Ax_k$ , where  $A$  is then chosen to minimize  $\|x_{k+1} - Ax_k\|_2$  over  $k = 1, 2, 3, \dots, n - 1$ . This linear system is shown in equation 2

$$dx/dt = f(x, t) \quad (2)$$

Now, as we have collected the data from the system, i.e.  $x_{k+1}$  and  $x_k$  are known, but the

function relating them is unknown as shown in equation 3

$$x_{k+1} = F(x_k) \quad (3)$$

DMD then constructs a locally linear approximation of the dynamical system shown in equation 4

$$\frac{dx}{dt} = Ax \quad (4)$$

This ordinary differential equation (ODE) form of the starting non-linear dynamical system is advantageous since, with given initial conditions, there is a well known solution for this system as shown in equation 5

$$x(t) = \sum_{k=1}^n \phi_k \exp(\omega_k t) b_k = \Phi \exp(\Omega t) \mathbf{b} \quad (5)$$

where  $b_k$  is the initial amplitude of each mode,  $\phi_k$  are the eigenvectors of  $A$  and  $\omega_k$  are the eigenvalues of  $A$ . Now, when the dimensions of  $X$  are large, it makes  $A$  extremely large to compute. The existing DMD process (as can be seen in current literature) circumvents this by the eigendecomposition of  $A$  by considering a rank reduced representation,  $\tilde{A}$ , by performing Singular Value Decomposition (SVD) of the collected data.

$$X \approx U \Sigma V^* \quad (6)$$

In equation 6,  $X$  is a rectangular data matrix of size  $m \times n$ ,  $U$  is a complex unitary matrix of size  $m \times n$  that contains the left singular vectors which are the POD modes,  $\Sigma$  is a rectangular diagonal matrix of size  $m \times n$  having positive real number as its diagonal elements and  $V^*$  is a complex unitary matrix of size  $n \times n$  and the superscript  $*$  represents a complex conjugate transform. The diagonal elements  $\sigma_i$  of  $\Sigma_{ij}$  are the singular values

of  $X$ . Next, the matrix  $A$  may be obtained by using the pseudo-inverse of  $X$ , shown in equation 7

$$A = X'V\Sigma^{-1}U^* \quad (7)$$

Note that, in practice, as  $A$  can be computationally prohibitive to calculate,  $\tilde{A}$  is computed by a unitary transform of  $A$  shown in equation 8

$$\tilde{A} = U^*AU = U^*X'V\Sigma^{-1} \quad (8)$$

With  $\tilde{A}$  we can now create a low dimensional subspace of  $A$

$$\tilde{x}_{k+1} = \tilde{A}\tilde{x}_k \quad (9)$$

We can now compute the eigendecomposition of  $\tilde{A}$

$$\tilde{A}W = W\Lambda \quad (10)$$

where columns of  $W$  are the eigenvectors and diagonal elements,  $\lambda_k$ , of  $\Lambda$  are the eigenvalues. Now we can use the eigendecomposition of  $\tilde{A}$  to reconstruct the eigendecomposition of  $A$ . The eigenvalues of  $A$ ,  $\omega_k$ , are given by the diagonal elements  $\lambda_k$  of  $\Lambda$  scaled logarithmically according to  $\omega_k = \ln(\lambda_k)/\Delta t$ . The eigenvectors of  $A$  are given by equation 11

$$\Phi = X'V\Sigma^{-1}W \quad (11)$$

The initial amplitudes may be calculated as

$$b = \Phi^\dagger x_1 \quad (12)$$

System state predictions now can be obtained using  $\phi_k$ ,  $\omega_k$  and  $b_k$  in equation 5. An interested reader is again directed to [42, 43, 27] for a more detailed description of the DMD process. Lastly, following Kou et al. [44], equation 5 can be rewritten as:

$$x_i = \sum_{j=1}^{N-1} b_{ij}\Phi_{\text{Norm},j}(x, y). \quad (13)$$

In equation 13 [44],  $\Phi_{\text{Norm},j}$  represents the  $j^{\text{th}}$  dynamic mode normalized by its Frobenius norm with subscript “Norm” representing the word “normalized”, and  $b_{ij}$  is the time coefficient of the  $j^{\text{th}}$  normalized mode at time instant  $i$  [44]. This representation was then used by Kou and Zhang [44] to extract a new parameter,  $I_j$ , which denotes the influence of a particular mode on the entire sampling window as opposed to only at the initial condition. The parameter  $I_j$  is defined in equation 14, and was proposed as an improved method of mode selection by Kou and Zhang [44].

$$I_j = \int |b_j(t)| \approx \int_{i=1}^N |b_{ij}| dt \quad (14)$$

However, in a subsequent paper, this concept was further modified by Ahani and Uddin [20], and the integral term was replaced by a Root Mean Squared (RMS) term. This new RMS method, as proposed by Ahani and Uddin [20], was used in this work for mode selection.

## 5 DMD PROCESS VALIDATION: APPLICATION OF DMD TO A CANONICAL FLOW

As a first learning exercise, and to validate our DMD data collection and post-processing tools, a DMD of the canonical flow past a 2D circular cylinder at a Reynolds number of 75 was performed, similar to a number of DMD fluid dynamics research found in literature [45]. The numerical setup used for this exercise is taken from the Star-CCM+ guide which references the work of Daily et al. [46]. It is a 2D incompressible, isothermal flow solved using the segregated URANS solver. In Fig 4, the normalized stream-wise velocity, labeled as VRX, from

the CFD and DMD are compared in which VRX from the CFD and DMD are shown in the top and middle figures, respectively. The bottom figure shows the difference,  $\Delta VRX$ , between the two, i.e.  $\Delta VRX$  is equal to the CFD computed VRX subtracted from the DMD predicted VRX. Note that time  $t$  is normalized by  $D * U_{Ref}$ , where  $D$  is the diameter of the cylinder and  $U_{Ref}$  is the reference freestream velocity. It is evident that the DMD reconstruction is well-correlated to the CFD prediction.

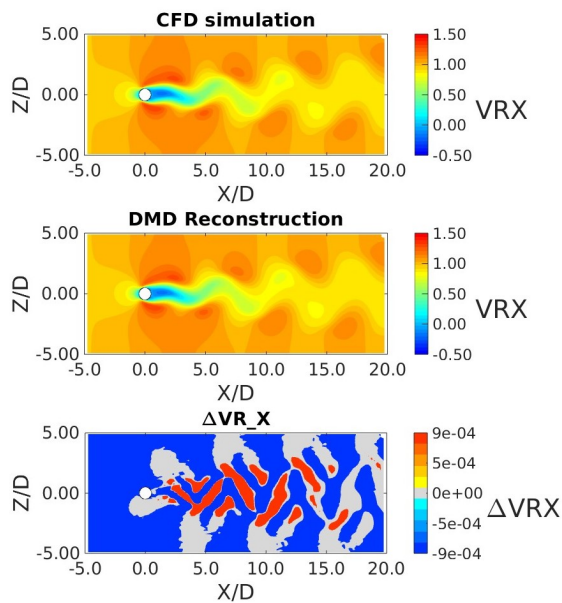


Figure 4: Comparison of CFD prediction and DMD reconstruction of normalized instantaneous stream-wise velocity for flow past a 2D cylinder at time  $t = 120$ .

Two issues require further consideration before the DMD of the flow past an Ahmed body at a high Reynolds number is attempted. Firstly, it is pointless to compare two instantaneous turbulent flows. Thus, the mean and fluctuating components are required to be addressed separately. This is illustrated, for the above 2D cylinder case, in Figures 5 and 6 which show a comparison the mean and fluctuating

components of the normalized stream-wise velocity fields as obtained from the CFD computations and DMD reconstructions.

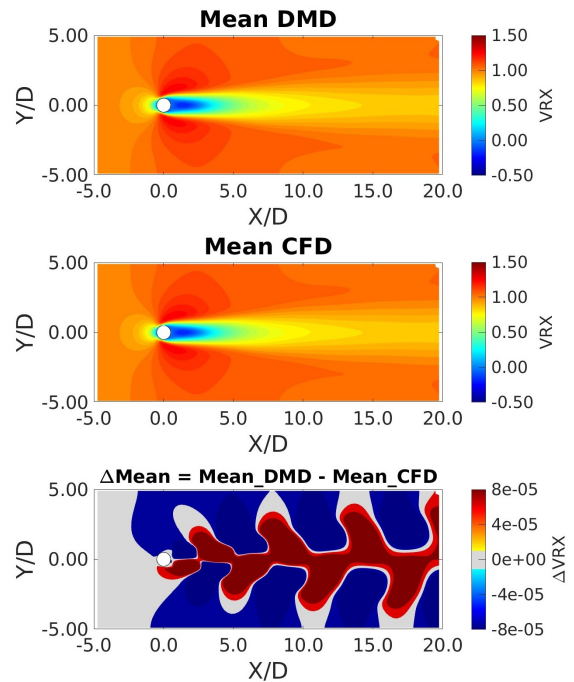


Figure 5: Mean stream-wise velocity component  $u(t)$  for the flow past a 2D circular cylinder.

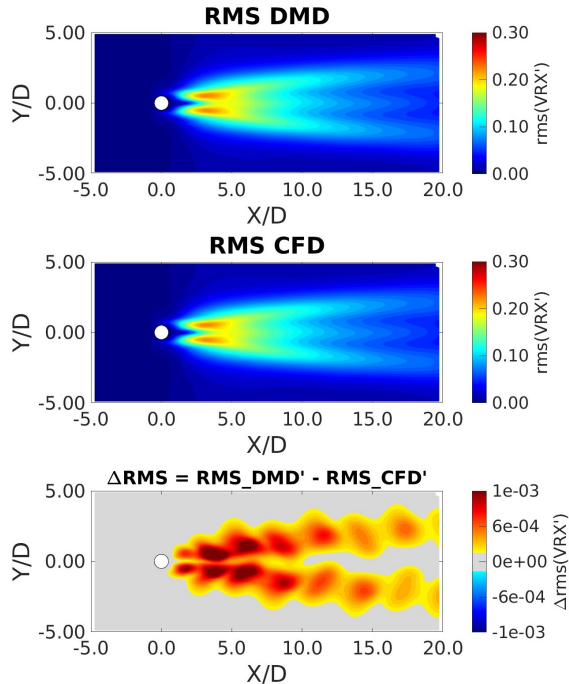


Figure 6: RMS of stream-wise velocity component  $u(t)$  for the flow past a 2D circular cylinder.

The other issue concerns the practicality of the data collection strategy. Storing time-series data from the entire volume of interest would require an enormous 3 petabytes of data to be recorded. Given that the focus of this work is on aerodynamic force and moment predictions of a GV, only the surface static pressure data over the Ahmed body would be required to be collected. However, keeping in mind future works involving the analyses of the flow field around the GV, seven scalar fields over ten reference planes around the Ahmed body were also collected. These scalar fields included: pressure coefficient, three components of velocity, turbulence kinetic energy (TKE), vorticity, and the  $Q$ -criteria. These planes were chosen using two criteria. Firstly, some of these planes, such as the wake planes at  $X/L = 1.077, 1.192,$  and  $1.479$ , have experimental data available, and

potentially can be used for future validation purposes. The other chosen planes were anticipated to exhibit interesting flow features in critical flow regimes when crosswind and vehicle interaction simulations would be performed in future investigations. These include: (a)  $y$ -planes at  $Y/W = 0.5, 0.88$  and  $1.27$ , and (b)  $z$ -planes at  $Z = 0.5 \times \text{Ground Clearance}, 0.5H, 1.15H,$  and  $1.3H$ . This strategy resulted in storing only 400 GB of data per GV simulation of which the surface static pressure data over the Ahmed body consists of only 40 GB of data - a much more practical approach.

## 6 RESULTS

### 6.1 Default DMD Approach

To help address the issues related to temporal resolution of the data collected for DMD analysis, the CFD time step size was reduced to  $\Delta t = 0.0001\text{s}$  and data for DMD was collected at 10 kHz sampling frequency as sampling at lower frequencies proved ineffective. Figs 7 and 8 show the CFD and DMD coefficients from the data, and illustrate that the fluctuating components have a noticeable improvement, while the nonphysical dampening rates remain. On the spectra, the DMD spectrum improved throughout the frequency range. Many of the characteristic low-frequency modes of the flow have been captured and the medium-frequency peaks were well resolved. However, there remains significant room for improvement.

### 6.2 Modified DMD Approach

To circumvent all issues discussed above, a modification to the commonly used DMD algorithm was made. The schematic for the proposed process is shown in Fig 9. Basically, the truncation step of the SVD was

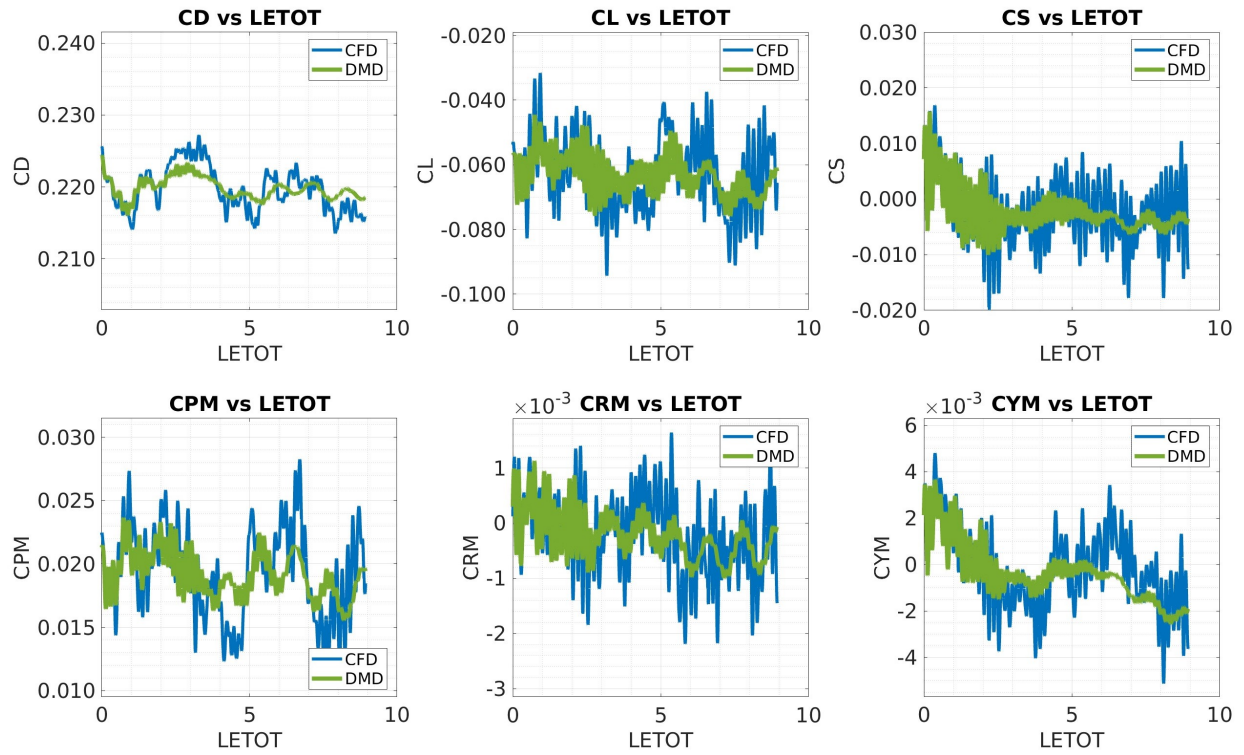


Figure 7: Forces and Moments of CFD vs DMD, sampled at 10 kHz

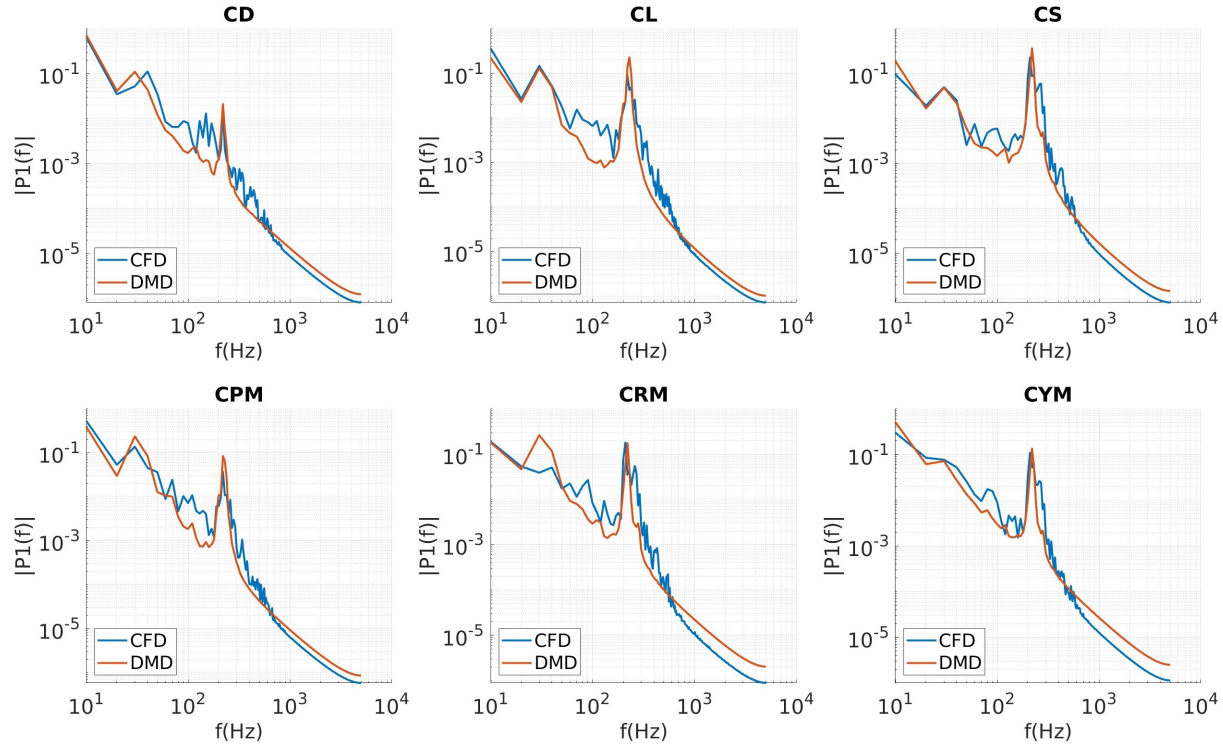


Figure 8: PSD of Forces and Moments of CFD vs DMD, sampled at 10 kHz

removed and custom filtering of the DMD modes was introduced. The filters examine the time dynamics associated with each mode and identify nonphysical modes based on their predicted amplitudes, frequencies, and contribution towards the total energy. This modified DMD process was then applied to the sampled data.

Like before, the force and moment coefficients for both the CFD and the DMD, and their PSDs were examined and presented in Figs 10 and 11, and a significant improvement was observed. The forces and moments reconstructed via DMD almost perfectly matched the CFD data, and the same can be observed in spectra. While there remains some room for improvement in the medium and high frequencies, the reader is reminded that the data was collected from an IDDES simulation, which cannot resolve

the very high-frequency flow characteristics. Thus, this limitation may be that of CFD, rather than DMD.

### 6.3 Coefficients of aerodynamic Forces and Moments

In order to investigate the effectiveness of DMD to predict force and moment coefficients, a comparison of these quantities obtained from the DMD reconstructed reduced order flow field against CFD predictions are presented in Table 1. Clearly, predictions from this method matched very well. Note that the CFD calculations to simulate 2 seconds of physical time required 14,400 CPU hours, whereas the DMD averaging over the same period took 15 seconds. In a future paper, investigating the effectiveness of the proposed ROM methods in predicting future events is of great interest.

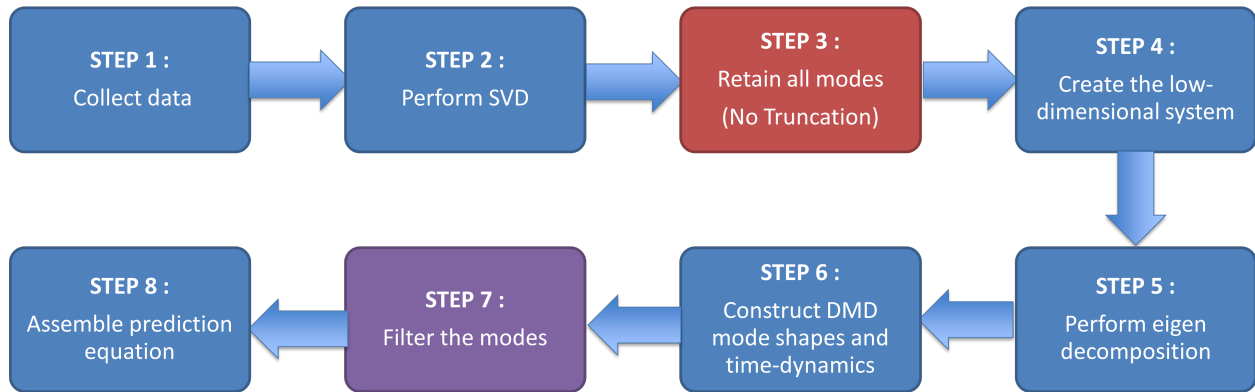


Figure 9: Schematic of the modified DMD algorithm

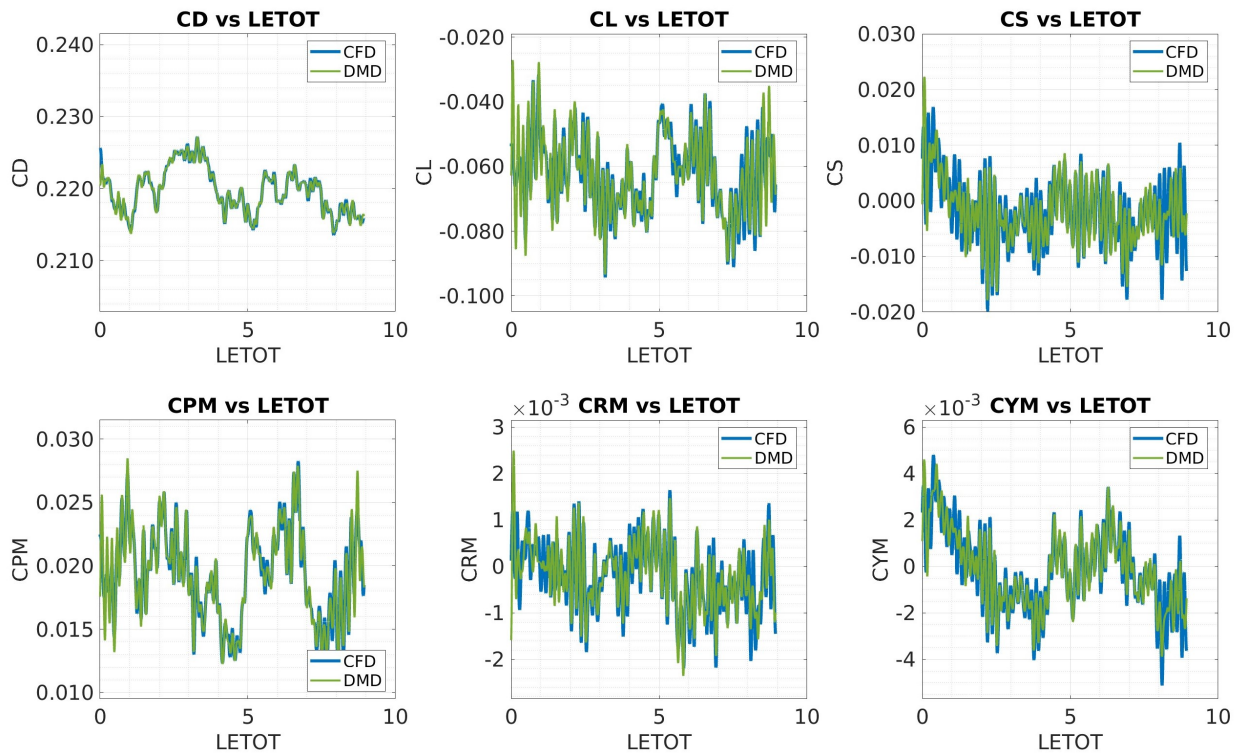


Figure 10: Forces and Moments of CFD vs DMD, sampled at 10kHz and using Custom Filters

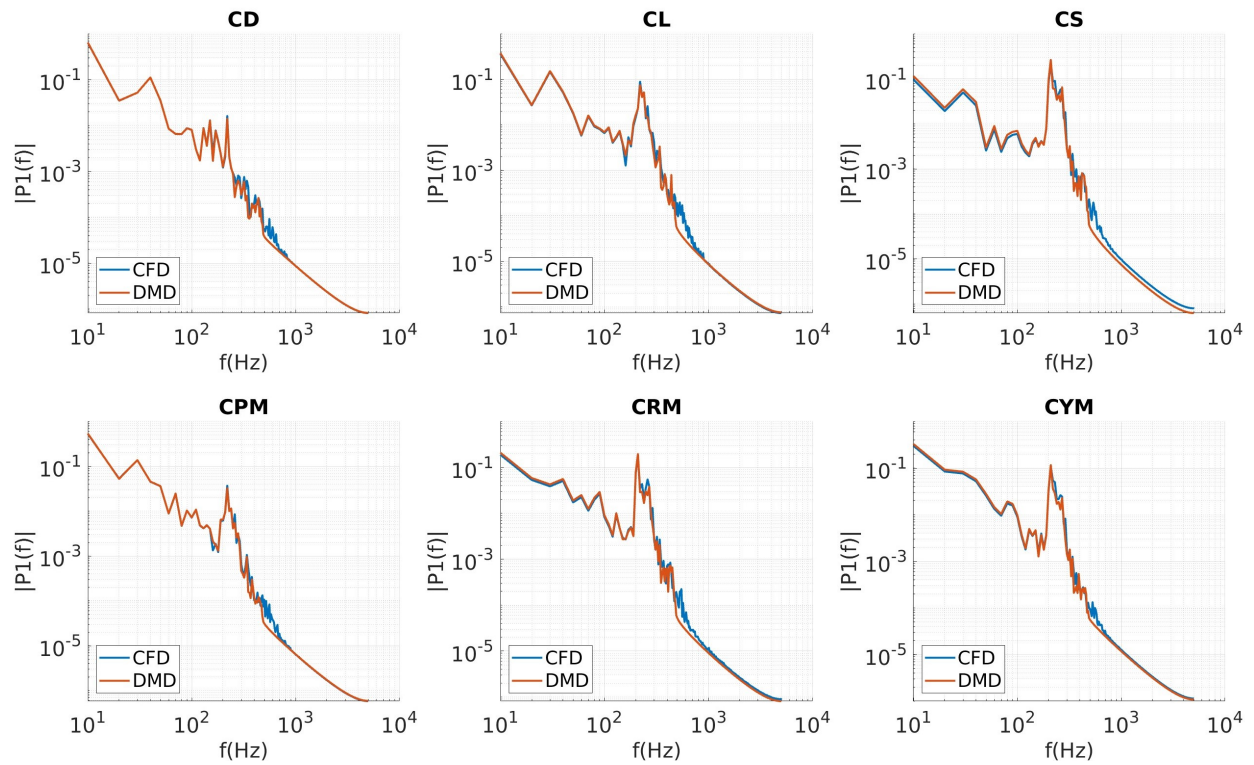


Figure 11: PSD of Forces and Moments of CFD vs DMD, sampled at 10kHz and using Custom Filters

	<b>CFD Mean</b>	<b>DMD Mean</b>	<b>CFD RMS</b>	<b>DMD RMS</b>
<b>CD</b>	0.220	0.220	0.003	0.003
<b>CL</b>	-0.062	-0.062	0.012	0.012
<b>CS</b>	-0.002	-0.002	0.006	0.006
<b>CPM</b>	0.019	0.019	0.004	0.004
<b>CRM</b>	0.000	0.000	0.002	0.001
<b>CYM</b>	0.000	0.000	0.001	0.002

Table 1: Coefficients of aerodynamic Forces and Moments as obtained from the full-blown CFD and DMD reconstructed reduced order flow-field.

## 7 CONCLUSION

This paper explored the adaptation of the Dynamic Mode Decomposition (DMD) algorithm to a high Reynolds number, separation-dominated flow over an idealized ground vehicle. The DMD algorithm in its existing form, as available from literature, was first applied to a low-Reynolds number flow past a 2D cylinder. Here the DMD reconstruction of the flow field was well correlated to the CFD simulation which was used to generate the data. The existing DMD algorithm was then applied to the moving GV flow where it failed to produce a DMD-based reduced order reconstruction of the flow field with sufficient accuracy. Investigation of the DMD matrices revealed that the DMD predictions were suffering from nonphysical dampening of the medium-to-high frequency modes. Subsequently, a modified DMD algorithm was proposed to overcome the deficiencies in the existing DMD algorithm for reconstruction of the flow field around the moving GV.

The modified DMD algorithm incorporated some crucial aspects to improve its performance. Firstly, it was shown that an IDDES-based CFD

simulation at a 10 kHz data sampling rate was sufficient to generate accurate and reliable DMD predictions. This was in contrast to traditional DMD-data gathering methods wherein either experimental data or DNS data is used. This data-gathering process was first validated by comparing the aerodynamic predictions from the IDDES-based CFD methodology against wind tunnel experiments and then validating the DMD reconstructed aerodynamic predictions against the known CFD data.

The second and third modifications involved the elimination of the truncation step in the SVD and the introduction of a custom-designed mode filtering process preceding the data reconstruction step. These modifications ensured that non-physical modes were removed from the reconstruction. The filters were based on the time dynamics of the mode, i.e. the mode amplitudes, frequencies, and growth rates. Using the same validation process as described earlier, the modified DMD algorithm was demonstrated to be capable of flow-field reconstruction that is correct to the accuracy of the CFD modeling scheme used to generate the training data.

Future work involves investigation of the modified algorithm's performance on its applicability to more complex flow phenomena such as predicting the interaction of flow fields of a platoon of vehicles, rotor-craft, and multiple road and/or aerial vehicles in close proximity. Further research is also required for the scientific optimization and refinement of the mode filtration process to ensure its robustness, computational efficiency, and exploring its potential for real-time flow control and optimization.

## 8. REFERENCES

### References

- [1] H. Tennekes, J. L. Lumley, J. L. Lumley *et al.*, *A first course in turbulence*. MIT press, 1972.
- [2] S. B. Pope and S. B. Pope, *Turbulent flows*. Cambridge university press, 2000.
- [3] K. Liu, B. Zhang, Y. Zhang, and Y. Zhou, “Flow structure around a low-drag ahmed body,” *Journal of Fluid Mechanics*, vol. 913, p. A21, 2021.
- [4] A. S. Misar, M. Uddin, A. Robinson, and C. Fu, “Numerical analysis of flow around an isolated rotating wheel using a sliding mesh technique.” SAE WCX Technical Paper 2020-01-0675, 2020.
- [5] M. Uddin, S. Nichols, C. Hahn, A. Misar, S. Desai, N. Tison, and V. Korivi, “Aerodynamics of landing maneuvering of an unmanned aerial vehicle in close proximity to a ground vehicle.” SAE Technical Paper 2023-01-0118, 2023.
- [6] M. Uddin, S. Mallapragada, and A. Misar, “Computational investigations on the aerodynamics of a generic car model in proximity to a side-wall.” SAE Technical Paper 2018-01-0704, 2018.
- [7] C. P. Bounds, S. Rajasekar, and M. Uddin, “Development of a numerical investigation framework for ground vehicle platooning,” *Fluids*, vol. 6, no. 11, p. 404, 2021.
- [8] J. Guo, X. Dong, Y. Gao, D. Li, and Z. Tu, “Simultaneous obstacles avoidance and robust autonomous landing of a uav on a moving vehicle,” *Electronics*, vol. 11, no. 19, p. 3110, 2022.
- [9] B. Zhang, K. Liu, Y. Zhou, S. To, and J. Tu, “Active drag reduction of a high-drag ahmed body based on steady blowing,” *Journal of Fluid Mechanics*, vol. 856, pp. 351–396, 2018.
- [10] C. Zhang, M. Uddin, X. Song, C. Fu, and L. Foster, “Simultaneous improvement of vehicle under-hood airflow and cooling drag using 3d cfd simulation,” SAE Technical Paper, Tech. Rep., 2016.
- [11] H. Lienhart and S. Becker, “Flow and turbulence structure in the wake of a simplified car model,” *SAE transactions*, pp. 785–796, 2003.
- [12] C. D. Argyropoulos and N. Markatos, “Recent advances on the numerical modelling of turbulent flows,” *Applied Mathematical Modelling*, vol. 39, no. 2, pp. 693–732, 2015.
- [13] A. Misar, “Insight into the aerodynamics of race and idealized road vehicles using scale-resolved and scale-averaged cfd simulations,” Ph.D. dissertation, The University of North Carolina at Charlotte, 2023.
- [14] A. S. Misar and M. Uddin, “Effects of solver parameters and boundary conditions on RANS CFD flow predictions over a Gen-6 NASCAR racecar.” SAE WCX Technical Paper 2022-01-0372, 2022.
- [15] B. Zhang, Y. Zhou, and S. To, “Unsteady flow structures around

- a high-drag ahmed body,” *Journal of Fluid Mechanics*, vol. 777, pp. 291–326, 2015.
- [16] B. Wang, Z. Yang, and H. Zhu, “Active flow control on the 25° ahmed body using a new unsteady jet,” *International Journal of Heat and Fluid Flow*, vol. 79, p. 108459, 2019.
- [17] C. Fu, C. Bounds, M. Uddin, and C. Selent, “Fine tuning the sst  $k-\omega$  turbulence model closure coefficients for improved nascar cup racecar aerodynamic predictions,” *SAE International Journal of Advances and Current Practices in Mobility*, vol. 1, no. 2019-01-0641, pp. 1226–1232, 2019.
- [18] A. S. Misar, M. Uddin, T. Pandaleon, and J. Wilson, “Scale-resolved and time-averaged simulations of the flow over a NASCAR cup series racecar.” SAE WCX Technical Paper Number 2023-01-0735, 2023.
- [19] A. Misar, P. Davis, and M. Uddin, “On the effectiveness of scale-averaged rans and scale-resolved iddes turbulence simulation approaches in predicting the pressure field over a nascar racecar,” *Fluids*, vol. 8, no. 5, p. 157, 2023.
- [20] H. Ahani, J. Nielsen, and M. Uddin, “The proper orthogonal and dynamic mode decomposition of wake behind a fastback driver model,” SAE Technical Paper, Tech. Rep., 2022.
- [21] A. Misar, N. A. Tison, V. M. Korivi, and M. Uddin, “Application of the dmd approach to high-reynolds-number flow over an idealized ground vehicle,” *Vehicles*, vol. 5, no. 2, pp. 656–681, 2023.
- [22] P. J. Schmid, “Dynamic mode decomposition of numerical and experimental data,” *Journal of fluid mechanics*, vol. 656, pp. 5–28, 2010.
- [23] P. J. Schmid, L. Li, M. P. Juniper, and O. Pust, “Applications of the dynamic mode decomposition,” *Theoretical and Computational Fluid Dynamics*, vol. 25, no. 1, pp. 249–259, 2011.
- [24] P. J. Schmid, D. Violato, and F. Scarano, “Decomposition of time-resolved tomographic piv,” *Experiments in fluids*, vol. 52, no. 6, pp. 1567–1579, 2012.
- [25] J. L. Proctor, S. L. Brunton, and J. N. Kutz, “Dynamic mode decomposition with control,” *SIAM Journal on Applied Dynamical Systems*, vol. 15, no. 1, pp. 142–161, 2016.
- [26] J. N. Kutz, S. L. Brunton, B. W. Brunton, and J. L. Proctor, *Dynamic mode decomposition: data-driven modeling of complex systems*. SIAM, 2016.
- [27] P. J. Schmid, “Dynamic mode decomposition and its variants,” *Annual Review of Fluid Mechanics*, vol. 54, pp. 225–254, 2022.
- [28] A. Wynn, D. Pearson, B. Ganapathisubramani, and P. J. Goulart, “Optimal mode decomposition for unsteady flows,” *Journal of Fluid Mechanics*, vol. 733, pp. 473–503, 2013.

- [29] P. J. Schmid, "Application of the dynamic mode decomposition to experimental data," *Experiments in Fluids*, vol. 50, pp. 1123–1130, 2011.
- [30] W. Mengmeng, H. Zhonghua, N. Han, S. Wenping, S. Le Clainche, and E. Ferrer, "A transition prediction method for flow over airfoils based on high-order dynamic mode decomposition," *Chinese Journal of Aeronautics*, vol. 32, no. 11, pp. 2408–2421, 2019.
- [31] R. Qiu, R. Huang, Y. Wang, and C. Huang, "Dynamic mode decomposition and reconstruction of transient cavitating flows around a clark-y hydrofoil," *Theoretical and Applied Mechanics Letters*, vol. 10, no. 5, pp. 327–332, 2020.
- [32] D. Matsumoto, L. Haag, and T. Indinger, "Investigation of the unsteady external and underhood airflow of the driver model by dynamic mode decomposition methods," *International Journal of Automotive Engineering*, vol. 8, no. 2, pp. 55–62, 2017.
- [33] S. R. Ahmed, G. Ramm, and G. Faltin, "Some salient features of the time-averaged ground vehicle wake," *SAE Transactions*, pp. 473–503, 1984.
- [34] M. Shur, P. Spalart, M. Strelets, and A. Travin, "A hybrid rans-les model with delayed des and wall-modelled les capabilities," *International Journal of Heat and Mass Transfer. To be published*, 2007.
- [35] F. R. Menter, "Two-equation eddy-viscosity turbulence models for engineering applications," *AIAA journal*, vol. 32, no. 8, pp. 1598–1605, 1994.
- [36] F. Menter, "Zonal two equation kw turbulence models for aerodynamic flows," in *23rd fluid dynamics, plasmadynamics, and lasers conference*, 1993, p. 2906.
- [37] E. Guilmineau, G. Deng, A. Leroyer, P. Queutey, M. Visonneau, and J. Wackers, "Assessment of hybrid rans-les formulations for flow simulation around the ahmed body," *Computers & Fluids*, vol. 176, pp. 302–319, 2018.
- [38] M. Aultman, Z. Wang, and L. Duan, "Effect of time-step size on flow around generic car models," *Journal of Wind Engineering and Industrial Aerodynamics*, vol. 219, p. 104764, 2021.
- [39] A. S. Misar, C. Bounds, H. Ahani, M. U. Zafar, and M. Uddin, "On the effects of parallelization on the flow prediction around a fastback driver model at different attitudes." SAE WCX Technical Paper 2021-01-0965, 2021.
- [40] C. Fu, M. Uddin, and C. Zhang, "Computational analyses of the effects of wind tunnel ground simulation and blockage ratio on the aerodynamic prediction of flow over a passenger vehicle," *Vehicles*, vol. 2, no. 2, pp. 318–341, 2020.
- [41] A. Altinisik, E. Kutukceken, and H. Umur, "Experimental and numerical

aerodynamic analysis of a passenger car: Influence of the blockage ratio on drag coefficient,” *Journal of Fluids Engineering*, vol. 137, no. 8, 2015.

- [42] D. Dylewsky, M. Tao, and J. N. Kutz, “Dynamic mode decomposition for multiscale nonlinear physics,” *Physical Review E*, vol. 99, no. 6, p. 063311, 2019.
- [43] J. H. Tu, “Dynamic mode decomposition: Theory and applications,” Ph.D. dissertation, Princeton University, 2013.
- [44] J. Kou and W. Zhang, “An improved criterion to select dominant modes from dynamic mode decomposition,” *European Journal of Mechanics-B/Fluids*, vol. 62, pp. 109–129, 2017.
- [45] M. Sakai, Y. Sunada, T. Imamura, and K. Rinoie, “Experimental and numerical flow analysis around circular cylinders using pod and dmd,” in *44th AIAA Fluid Dynamics Conference*, 2014, p. 3325.
- [46] J. W. Daily, W. James, D. R. Harleman *et al.*, *Fluid dynamics*. Addison-Wesley, 1966.